Richards, Iona; Houlsby, Guy; Byrne, Byron

Exploring the Response of a Monopile to Storm Loading

Coastal Structures 2019 - Nils Goseberg, Torsten Schlurmann (eds) - © 2019 Bundesanstalt für Wasserbau
ISBN 978-3-939230-64-9 (Online) - DOI: 10.18451/978-3-939230-64-9_095

Exploring the Response of a Monopile to Storm Loading

I. A. Richards, G. T. Houlsby & B. W. Byrne
Department of Engineering Science, University of Oxford

Abstract: Monopile foundations support the vast majority of offshore wind turbines in Europe. These foundations experience cyclic lateral loading caused by wind and waves. Many physical modelling studies have explored the response of monopiles to unidirectional, constant amplitude cyclic loading, but few have focused on the response during a realistic storm, where cyclic loading varies in amplitude, frequency and direction. In this paper, realistic storm loading, derived from wave loading tests performed as part of the DeRisk project, is applied to a laboratory scale monopile. The laboratory scale response informs calibration of a basic numerical model which, when coupled with appropriate scaling methods, allows prediction of the prototype scale response. Focus is placed on the inter-disciplinary methodology employed.

Keywords: Monopile foundation, cyclic loading, wave-structure interaction, physical modelling

1 Introduction

The offshore wind industry has grown rapidly in recent years and expansion is expected to continue: by 2030 Europe is projected to have 70 GW of installed offshore wind capacity (Wind Europe 2018). The majority of offshore wind turbines (OWTs) are supported on monopile foundations, which now have diameters 6 – 8 m (*e.g.* Sørensen et al., 2017), but with even larger diameters under consideration for the future. OWT structures are subjected to significant lateral loads, predominantly caused by wind and waves. The resulting combined horizontal and moment loading experienced by the foundation is cyclic in nature, but continually varies in amplitude, frequency and direction. Established design methods are not able to capture adequately the response of a monopile to this complex loading history, and new design methods are necessary for the next generation of monopiles.

Physical modelling at both 1g and in the centrifuge has provided valuable insights into the response of monopiles. Most of the research addresses unidirectional, constant amplitude cyclic loading (*e.g.* Leblanc et al. 2010, Klinkvort & Hededal 2013, Truong et al. 2018, Abadie et al. 2018). These studies have shown how monopiles accumulate rotation, and that their stiffness and damping properties may change with repeated cyclic loading at non-zero mean load. These studies have also informed the development of various methods for predicting the ratcheting behaviour of monopiles (e.g. Achmus et al. 2009, Houlsby et al. 2017, Bayton et al. 2018), but no method is yet widely accepted for prototype scale design.

This paper demonstrates how laboratory scale testing can be used to inform model development and prediction of the prototype scale response of a monopile, when coupled with appropriate scaling methods. Focus is placed on exploring the response of monopiles to realistic storm loading, derived from wave loading tests performed as part of the DeRisk project (Bredmose et al. 2016). While unidirectional, constant amplitude cyclic loading allows systematic exploration of the fundamental response of a monopile, applying representative storm loading (which varies in amplitude, frequency and direction) provides new insights into the response of monopiles to realistic loading, and provides validation data for model development.

2 Methodology

Fig. 1 summarises the inter-disciplinary methodology employed to explore the response of a monopile foundation to storm loading; relevant section titles of this paper are shown in italics. Model scale wave loading tests, performed as part of the DeRisk project (Bredmose et al. 2016), provide wave loads on a rigid monopile, appropriately scaled to prototype values. These prototype wave loads are processed to account for dynamic effects for a non-rigid monopile, and are then projected to a constant load eccentricity. These prototype environmental loads are then scaled and applied to the geotechnical model. The response of the geotechnical model informs calibration of a simple (multi-surface kinematic hardening) numerical model, which is scaled to a prototype design and used to predict the response of the prototype monopile to storm loading.

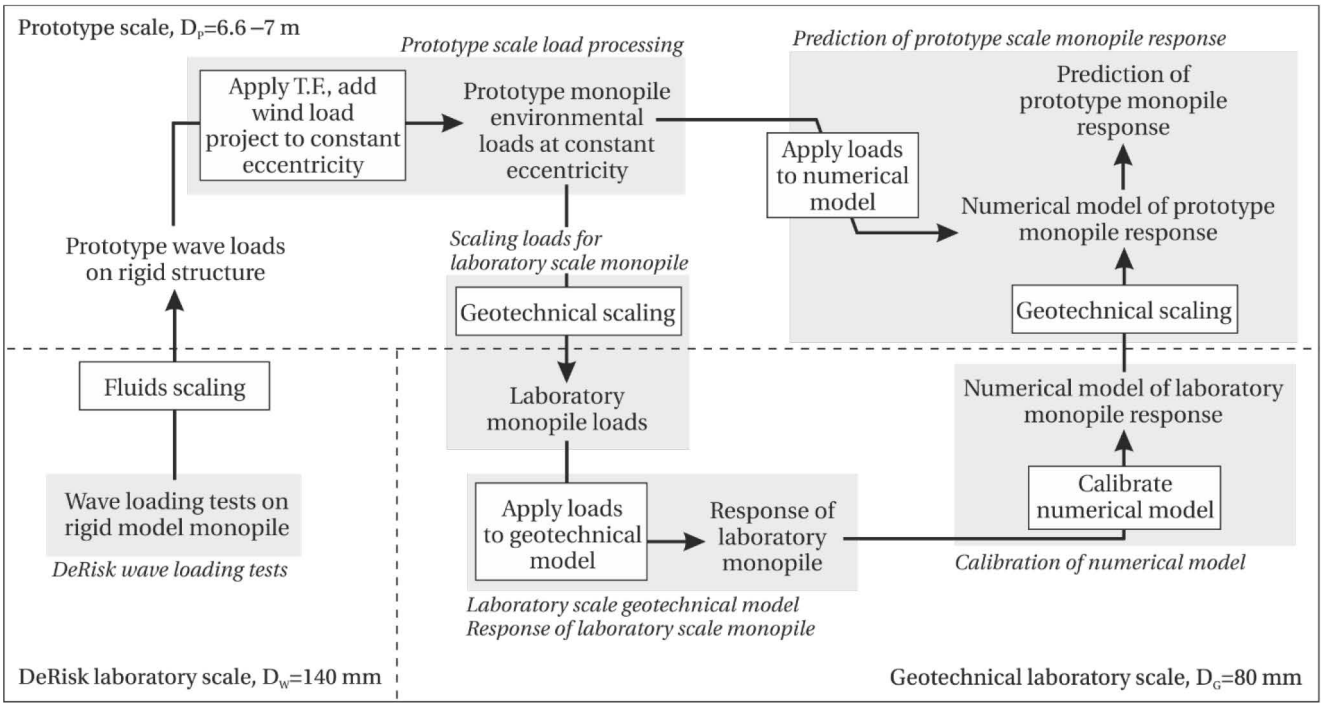

Fig. 1. Methodology employed to explore the response of monopiles to storm loading.

3 DeRisk wave loading tests

The prototype wave loads used in this study were derived from model-scale wave loading tests performed at the Danish Hydraulic Institute (DHI), as part of the multi-centre DeRisk project, which focused on reducing the risk associated with predicting ULS wave loads on OWT structures (Bredmose et al. 2016). The DeRisk tests were performed at 1:50 scale in a shallow water wave basin, representing a prototype monopile with diameter $D_P = 7$ m in the water column. The monopile was modelled by a stiff cylinder ($D_W = 140$ mm) instrumented with (amongst other instruments) four load cells for resolution of the total horizontal and moment load applied to the cylinder in two orthogonal directions. A range of wave conditions were generated, representative of large waves in severe storms in the North Sea (Bredmose et al. 2016).

The loading adopted for this paper is derived from a directionally spread test conducted in 33 m (prototype equivalent) water depth with peak spectral period 15 s and significant wave height 9.5 m at prototype scale, approximately corresponding to a 100 year return period. The spread angle $\Phi = 22°$. Using measured wave loads introduces non-Gaussian skewness in loads that is representative of loading in the field. Wave skewness affects mean wave load and peak wave load, both of which play a key role in determining the monopile response. Many simplified wave model will underestimate wave skewness (*e.g.* Wang 2018) and linear models will predict symmetric waves.

4 Laboratory scale geotechnical model

The geotechnical model is central to the exploration of the response of the monopile to storm loading. The cyclic loading apparatus described by Richards et al. (2018), and shown in Fig. 2, is used to explore the response of the monopile to lateral loading. Two electric actuators apply multidirectional lateral load to the monopile at an elevation h = 800 mm above the ground surface under load control, while six displacement transducers allow resolution of the position of the pile in six degrees of freedom. A rigid hollow aluminium pile is used with diameter $D_G = 80$ mm and a small length to diameter ratio ($L/D = 4$), representative of current full scale designs. Table 1 summarises the pile geometry.

The tests were conducted in Yellow Leighton Buzzard 14/25 sand, with properties summarised in Table 2. Tests were conducted in dry sand to simulate fully drained conditions, and samples were prepared by air pluviation to an average relative density $D_R = 60\%$. Following sample preparation, the model monopile was driven to the target embedment manually using a gravity hammer. Storm tests similar to those reported here were performed with the same set-up in very loose sand and reported by Richards et al. (2019a).

Tab. 1. Geotechnical model pile geometry

Pile diameter	D	80 mm
Pile embedded length	L	320 mm
Pile wall thickness	t	5 mm
Load eccentricity	h	800 mm

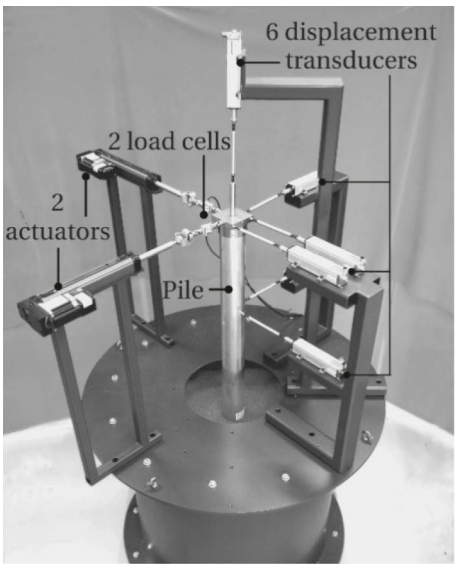

Fig. 2. Cyclic loading apparatus.

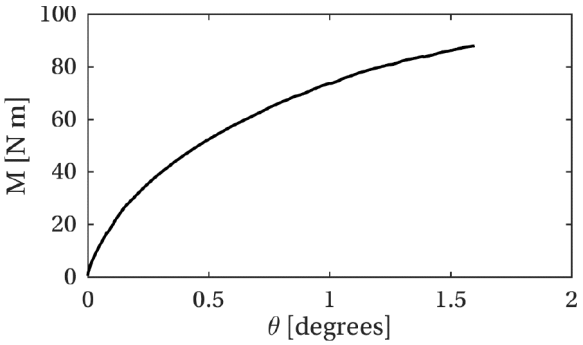

Fig. 3. Typical monotonic response of monopile.

Tab. 2. Yellow Leighton Buzzard 14/25 sand properties

Particle sizes	$D_{10}, D_{30}, D_{50}, D_{60}$	0.56, 0.69, 0.81, 0.87	mm
Maximum unit weight	γ_{MAX}	17.64	kN/m^3
Minimum unit weight	γ_{MIN}	14.43	kN/m^3
Critical friction angle (Schnaid 1990)	ϕ_{cr}	34.3	°

The strength of sand, characterised by its peak friction angle ϕ'_p, varies with mean effective stress level and relative density (Bolton 1986). Relative densities at laboratory scale (low stress level) generally represent higher relative densities at prototype scale, if sand strength is matched. However, the dilatant behaviour of sand (which controls ϕ'_p) is poorly understood at low stress-levels: Bolton (1986) proposes dilation increasing at low stress-levels, while other studies support a dilation limit (Bolton 1987, Tatsuoka et al. 1986, White 2018). Using the relationships proposed by Bolton (1986) and Bolton (1987), upper and lower estimates for the equivalent prototype density $D_{R,P}$ are obtained by equating model-scale and full-scale peak friction angle ϕ'_p. If the vertical effective stress at 70% pile embedment ($\sigma'_v = 0.7\gamma' L$) is chosen as a representative stress then the laboratory testing equates to a field relative density in the range of $64\% \leq D_{R,P} \leq 109\%$ ($40° \leq \phi'_p \leq 47°$).

The typical response of the model monopile to monotonic loading is shown in Fig. 3. The response is highly non-linear and does not reach a clear failure, as is typical for laterally-loaded monopiles. At an arbitrary reference rotation of $\theta_R = 2°$, broadly consistent with Abadie (2018) and Arshad & O'Kelly (2017), the reference moment capacity is (extrapolated to) $M_R = 95$ Nm.

5 Prototype scale load processing

Prototype scale wave loads were provided in terms of moment M and horizontal load H components in the I- and II-directions, where the I- direction is the principal loading direction. For conciseness, the first 3.4 hours of prototype scale wave data is used in the tests presented here; the full DeRisk tests represent 70 hours.

Fig. 4-a presents the prototype scale moment loads before the modifications discussed below are applied. To more realistically represent the environmental loading experienced by a prototype monopile a transfer function is applied to model the dynamic response of the flexible OWT structure (Fig. 4-b and Section 5.1.1). Constant wind load is added (Fig. 4-c and Section 5.1.2), and finally the loads are projected to a constant load eccentricity (height of load application point above ground level) to allow straightforward application with the available laboratory testing equipment (Fig. 4-d and Section 5.1.3).

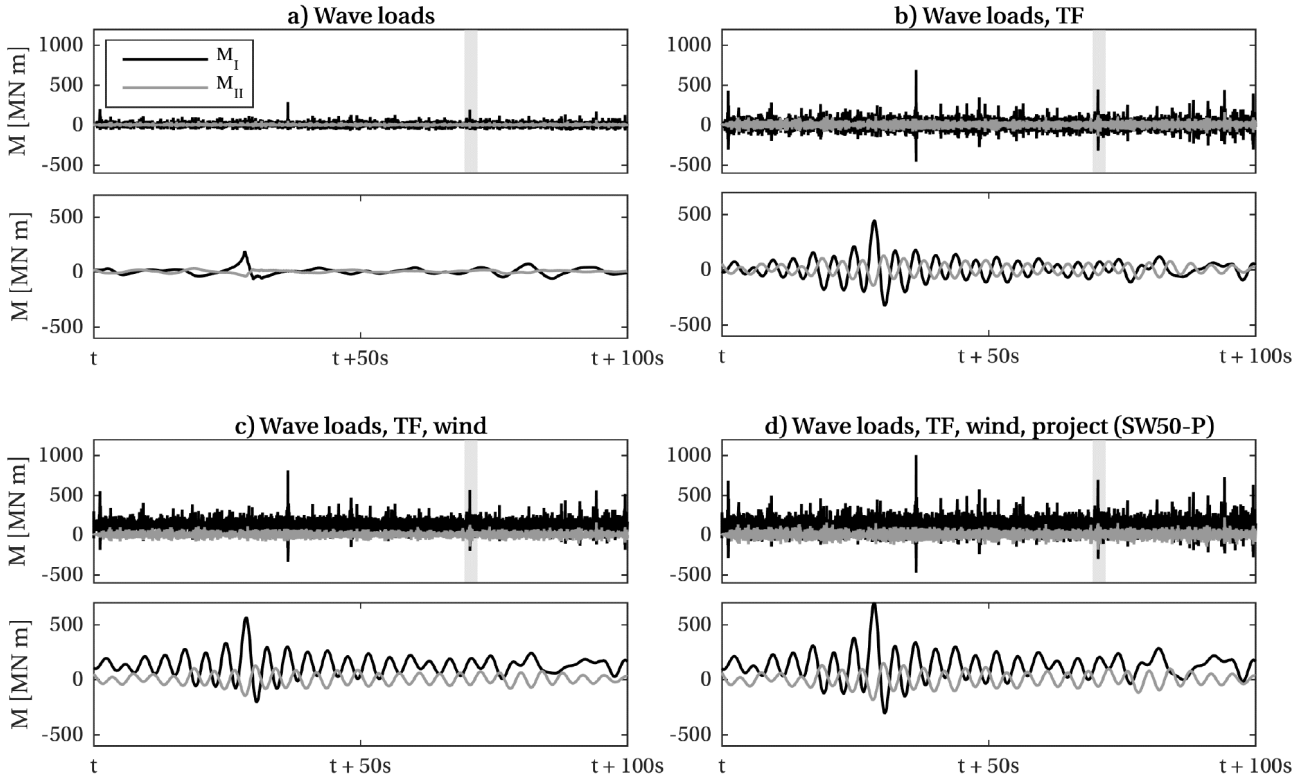

Fig. 4. Prototype scale storm moment loading time series. Upper plots present 3.4 hours of data (no scale on the x-axis); grey areas indicate region in lower plots, which highlight 100 seconds of data.

5.1.1 Application of transfer function to capture structural dynamics

A transfer function (TF) is applied to the loads to capture the dynamic response of the OWT structure. This process is necessary as the DeRisk tests were performed on a very stiff cylinder, with negligible dynamic amplification of loads. The OWT structure is approximated as a single degree of freedom system with a natural frequency f_0 and damping ratio ξ. For such a system the ratio of transmitted force F to excitation force P can be found as:

$$\frac{F}{P} = \frac{1}{\sqrt{\left(1-\left(\frac{f}{f_0}\right)^2\right)^2+\left(2\xi\frac{f}{f_0}\right)^2}} \quad (1)$$

Whilst dynamic amplification of loads will also occur at higher frequency modes (e.g. second tower bending mode and blade bending modes) this simple transfer function captures the key dynamic behaviour of the OWT, and has been used by e.g. Arany et al. (2017).

The first natural frequency of the prototype structure is estimated as $f_0 = 0.26$ Hz, between the 1P and 3P excitation frequencies for a Vestas V164-8.0MW turbine (University of Strathclyde, 2015). For parked conditions, where aerodynamic damping is negligible, the total damping is estimated as $\xi = 0.65\%$. However, there is much variation in damping ratio values reported in the literature, and damping varies with turbine operation conditions (Devriendt & Weijtjens, 2015).

The TF is approximated by an arbitrary magnitude filter and applied in the frequency domain. Fig. 5 shows the impact of the TF on the frequency content of the prototype wave loads (M_I), while Fig. 4-b, compared to Fig. 4-a, shows the impact of the TF on the moment loads in the time domain. The close proximity of prototype natural frequency ($f_0 = 0.26$ Hz) to the wave frequency content, coupled with the low damping ratio, leads to significant amplification of steep (higher frequency) wave loads. Peak loads approximately double and the number of cycles increases by around 50%. The impact of this TF is consistent with the experimental observations of Bachynski et al. (2017) who used an appropriately flexible monopile to explore dynamic amplification of wave loads.

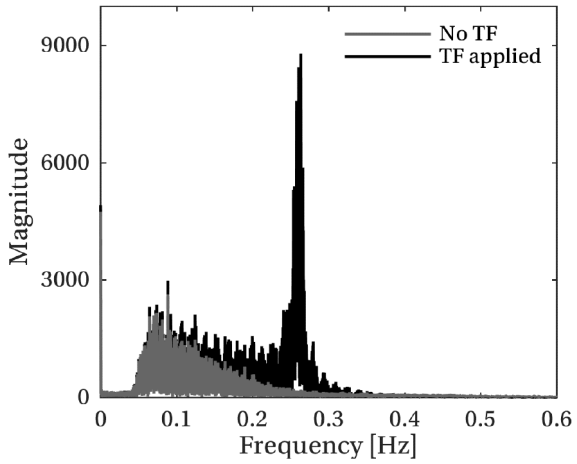

Fig. 5. Impact of transfer function (TF) on frequency content of M_I.

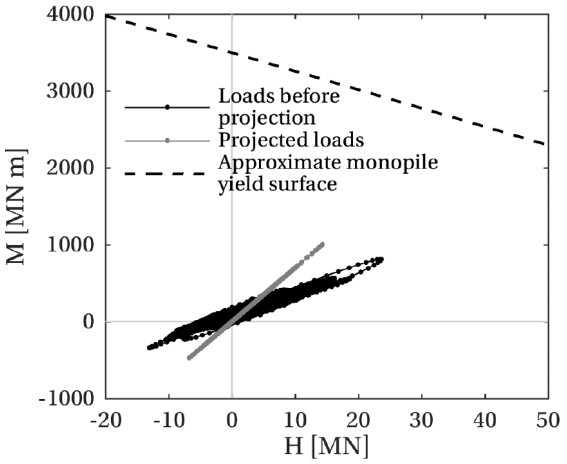

Fig. 6. Illustration of load projection in I-direction, for case including wind loading.

5.1.2 Addition of wind loading

Approximate wind loading is added to the prototype wave loads to better represent combined environmental loading. Given that the DeRisk test represents extreme storm conditions, the turbine is assumed to be parked with turbine blades feathered. A wind load of 1.4 MN acting at a height 85.5 m above mudline is estimated, assuming appropriate OWT dimensions and a 50-year design wind speed of 50 m/s. The relatively low-frequency variations in wind amplitude are neglected and the wind load is approximated as a constant load. Wind loading is aligned with the dominant wave loading direction. Throughout, the monopile response with and without wind loading is explored. Fig. 4-c presents the prototype scale moment time series with the additional wind loading.

5.1.3 Projection of loads to constant eccentricity

The measured wave loads have a variable eccentricity ($e = M/HD$). For loads to be applied to the laboratory scale monopile and to the simple numerical model, a constant loading eccentricity is required. Loads are projected onto a 'load-line' in $M - H$ space, with gradient representative of the loading eccentricity of the geotechnical laboratory set-up ($e = 10$), in a direction parallel to a simplified monopile yield surface. An approximate expression for a monopile yield surface is obtained by assuming a distributed lateral load per unit length of $DK\gamma' z$, taking $K = 3K_p$ (Broms, 1964) and linearising the yield surface in the region of interest (where M/H is positive):

$$\frac{M}{0.29K_pL^3D\gamma'} + \frac{H}{0.39K_pL^2D\gamma'} = 1 \tag{2}$$

The I- and II-direction components are projected independently. Fig. 6 illustrates the process of projecting the loads, while Fig. 4-d shows the small impact on the amplitude of moment loads. It is noted that the eccentricity of the geotechnical laboratory set-up is somewhat larger than that measured in the DeRisk tests, even after addition of wind loading.

The processed prototype scale loading presented in Fig. 4-d, with wind load, is referred to as SW50-P (Storm with $50\ \mathrm{m/s}$ Wind). The equivalent loading without wind load is referred to as SW0-P (Storm with $0\ \mathrm{m/s}$ Wind). The estimated loads at prototype scale were further factored by a safety factor of 1.35 for design purposes. Key load values at prototype scale are summarised in Table 3.

Tab. 3. Prototype scale signals

Signal name	Approx. number of cycles	Unfactored loads [MN m]				Loads factored by 1.35 [MN m]			
		I-direction (M_I)		II-direction (M_{II})		I-direction (M_I)		II-direction (M_{II})	
		Peak moment	Mean moment	Peak moment	Mean moment	Peak moment	Mean moment	Peak moment	Mean moment
SW0-P	2250	886	4.19	223	3.66	1196	5.66	301	4.94
SW50-P	2250	1003	121	223	3.66	1354	163.5	301	4.94

6 Scaling loads for laboratory scale monopile

The prototype environmental loads must be scaled down for application to the geotechnical model. The dimensionless framework presented by Leblanc et al. (2010) was used to bring together the response of monopiles in identical set-ups across a large stress-level range (Richards et al. 2019b), and a similar framework was used to compare laboratory and field tests on caissons (Kelly et al. 2006). Therefore, there is confidence in the use of this framework for scaling between laboratory and prototype scale. The key dimensionless groups are summarised in Table 4.

Tab. 4. Key dimensionless groups (Leblanc et al. 2010)

Moment	$\widetilde{M} = \dfrac{M}{L^3 D \gamma'}$
Rotation	$\tilde{\theta} = \theta \sqrt{\dfrac{p_a}{L\gamma'}}$

Tab. 5. Parameters for use in scaling

	Geotechnical laboratory scale	Prototype scale	Units
L	0.320	26.4	m
D	0.080	6.6	m
γ'	16.20	10.00	$\mathrm{kN/m^3}$

Moment and rotation scaling factors (f_M, f_θ) can be derived from the dimensionless groups (Eq. (3) and Eq. (4)), in terms of laboratory (L) and prototype (P) parameters presented in Table 5. The prototype L/D ratio is chosen to match the laboratory monopile, while the prototype effective unit weight γ' is estimated as $10\ \mathrm{kN/m^3}$ for a dense, saturated sand offshore.

$$f_M = \frac{M_P}{M_L} = \frac{L_P^3 D_P \gamma_P'}{L_L^3 D_L \gamma_L'} = 28.6 \times 10^6 \tag{3}$$

$$f_\theta = \frac{\theta_P}{\theta_L} = \sqrt{\frac{L_P \gamma_P'}{L_L \gamma_L'}} = 7.14 \tag{4}$$

This scaling approach generates peak laboratory scale loads (including the safety factor of 1.35) in the I-direction of $41.8\ \mathrm{Nm}$ and $47.4\ \mathrm{Nm}$, for SW0-L and SW50-L respectively. The finite response time of the load control system means the actual applied loads differ very slightly from the calculated values; the applied values are summarised in Table 6.

Tab. 6. Laboratory scale geotechnical test programme

Signal name	Approximate number of cycles	Applied loads I-direction (M_I) [Nm]		Applied loads II-direction (M_{II}) [Nm]	
		Peak moment	Mean moment	Peak moment	Mean moment
SW0-L	2250	39.9	0.08	10.6	0.23
SW50-L	2250	47.0	7.28	10.6	0.23

7 Response of laboratory scale monopile

The response of the laboratory scale monopile to storm loading is presented in Fig. 7. Fig. 7-a and Fig. 7-b show the moment-rotation response in the principal loading direction without and with additional wind loading; the monotonic response (backbone curve) is shown dashed. Fig. 7-c shows the rotation at cycle peaks (θ_P) against cycle number. The shape of the moment-rotation response in two arbitrary time periods (indicated by shaded regions in Fig. 7-c) is highlighted in black in Fig. 7-a and Fig. 7-b. The hysteretic response is characteristic of kinematic hardening.

The response is dominated by the large load events, and tends to follow the backbone curve when loads exceed those previously applied. However, the addition of wind loading (SW50), and associated increase in mean load, leads to significant accumulation of pile rotation, or ratcheting, in the I-direction.

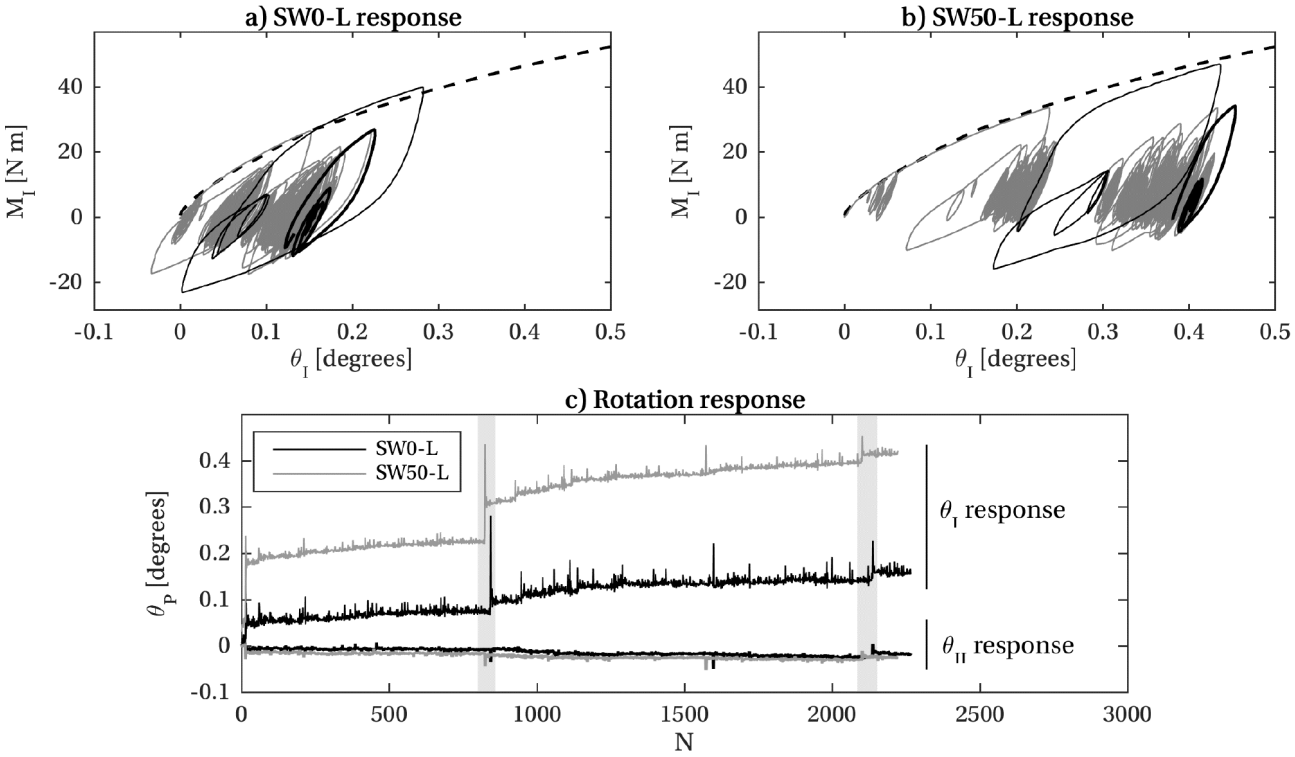

Fig. 7. Response of laboratory scale monopile to storm loading (backbone shown dashed in (a) and (b)).

8 Calibration of numerical model

The pile-soil system is represented by a macro model relating the global overturning moment to the corresponding monopile rotation, rather than by using a three-dimensional finite element model for the soil and pile. Multi-surface kinematic hardening macro models have been used to capture the hysteretic response of caisson (Nguyen-Sy & Houlsby, 2005) and monopile (Page et al., 2018) foundations. A key advantage of kinematic hardening models is that they operate implicitly and therefore multi-amplitude load signals do not require "rain-flow counting". Houlsby et al. (2017) also presented models derived from multi-surface kinematic hardening models, formulated in the hyperplasticity framework, which are able to capture ratcheting behaviour with the inclusion of a ratcheting element. Abadie et al. (2019) and Beuckelaers (2017) demonstrated the ability of these models to capture the monopile's response to cyclic lateral loading at model-scale and field-scale, respectively.

As this paper is focused on methodology, a basic kinematic hardening model, which provides the basis for the ratcheting models developed by Houlsby et al. (2017), is employed. The model is expressed in terms of conjugate stress σ and strain ε variables, which here represent applied moment M and pile rotation θ. Although the storm loading is multidirectional, Fig. 7-c shows negligible displacement in the II-direction, and a unidirectional model is used to approximate the response in the I-direction only.

The model employs N_s yield surfaces, with a strength k_n, stiffness H_n and plastic strain α_n associated with each surface, as shown in Fig. 8. The model is fully described by the Helmholtz free energy f and dissipation d functions (Puzrin & Houlsby 2001):

$$f = \frac{H_0}{2}\left(\varepsilon - \sum_{n=1}^{N_s} \alpha_n\right)^2 + \sum_{n=1}^{N_s} \frac{H_n}{2}\alpha_n^2 \tag{5}$$

$$d = \sum_{n=1}^{N_s} k_n|\dot{\alpha}_n| \tag{6}$$

Standard derivations, as described by Puzrin & Houlsby (2001), lead to specification of the constitutive behaviour, which may be implemented numerically in incremental from.

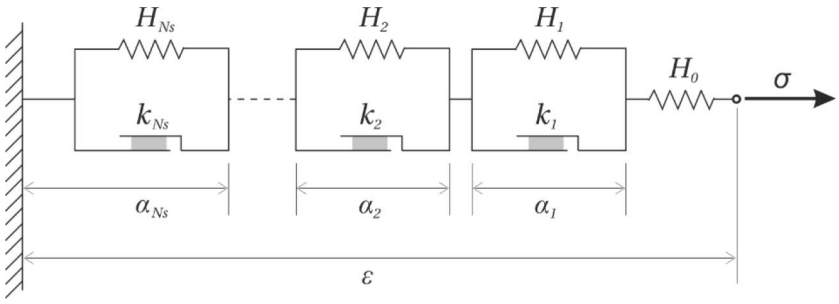

Fig. 8. Representation of multi-surface kinematic hardening model, after Houlsby et al. (2017).

The model is calibrated by specification of parameters H_0 (initial stiffness), H_n and k_n, which are derived from N_s points on the backbone curve $(\sigma_n, \varepsilon_n)$ following Houlsby et al. (2017). Here, the backbone curve is determined by fitting an analytical function to the experimental monotonic response shown in Fig. 3. Although σ_n, ε_n can be obtained directly from the experimental data, specification of a function for the backbone curve ensures smoothness of the model parameters (H_n, k_n) and facilitates later scaling. The plastic *p-y* expression presented by Jeanjean et al. (2017) is modified to include an elastic component and applied here to the global foundation response (Eq. (7)). A good fit to the monotonic curve in Fig. 3 is obtained with the parameters given in Table 7.

$$\varepsilon = \frac{\sigma}{E_i} + \left(\varepsilon_R - \frac{\sigma_R}{E_i}\right)\left(\frac{\operatorname{atanh}\left(\frac{\sigma}{\sigma_R}\tanh(A)\right)}{A}\right)^2 \tag{7}$$

Tab. 7. Laboratory scale backbone parameters

σ_{RL}	ε_{RL}	E_{iL}	A_L
95 Nm	2°	1217 Nm/°	0.853

Tab. 8. Prototype scale backbone parameters

$\sigma_{RP} = f_M\sigma_{RL}$	$\varepsilon_{RP} = f_\theta\varepsilon_{RL}$	$E_{iP} = (f_M/f_\theta)E_{iL}$	$A_P = A_L$
2717 MNm	14.3°	4877 MNm/°	0.853

Fig. 9 presents the kinematic hardening model predictions with $N_s = 100$, calibrated to a backbone curve described by Eq. (7) and the parameters presented in Table 7. The kinematic hardening model captures the rotation at peak load well, and broadly captures the shape of the hysteresis loops. However, the model does not capture the ratcheting behaviour, which is most significant in test SW50. To capture the ratcheting behaviour, a more advanced model, such as those developed by Houlsby et al. (2017) and demonstrated by Abadie et al. (2019) and Beuckelaers (2017) would be necessary.

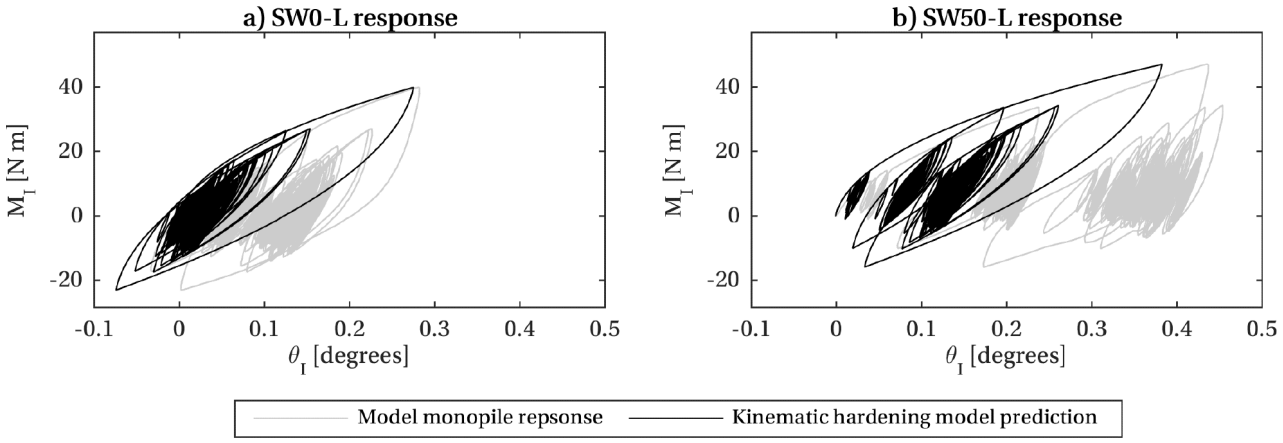

Fig. 9. Prediction of laboratory scale monopile response to storm loading, using kinematic hardening numerical model.

9 Prediction of prototype scale monopile response

To explore how a prototype monopile may respond to storm loading, the laboratory scale numerical model is scaled-up using the dimensionless framework proposed by Leblanc et al. (2010) (Table 4). The moment and rotation factors (f_M, f_θ) derived in Section 6 are applied to the laboratory scale backbone parameters to find prototype scale backbone parameters for a 6.6 m diameter, 26.4 m long monopile, as shown in Table 8. The kinematic hardening model parameters (H_0, H_n, k_n) are then re-calibrated to the prototype scale backbone.

The prototype scale numerical model is used to predict the response to I-direction prototype scale loads SW0-P and SW50-P, both unfactored and factored (safety factor = 1.35) (Table 3). Fig. 10 presents the predicted monopile response. With the loads factored, the transient rotation at peak load is 2.2° for SW0-P and 2.8° for SW50-P, but with the expected loads applied (unfactored) the rotations at peak load reduce to 1.2° and 1.5° respectively. Because of the non-linearity of the monopile response, factors of safety on load result in much greater factors on monopile rotation.

The response of a 6.6 m diameter, 26.4 m long monopile is explored here, but numerical models for alternative prototype monopile geometries could be generated straightforwardly by derivation of alternative moment and rotation factors.

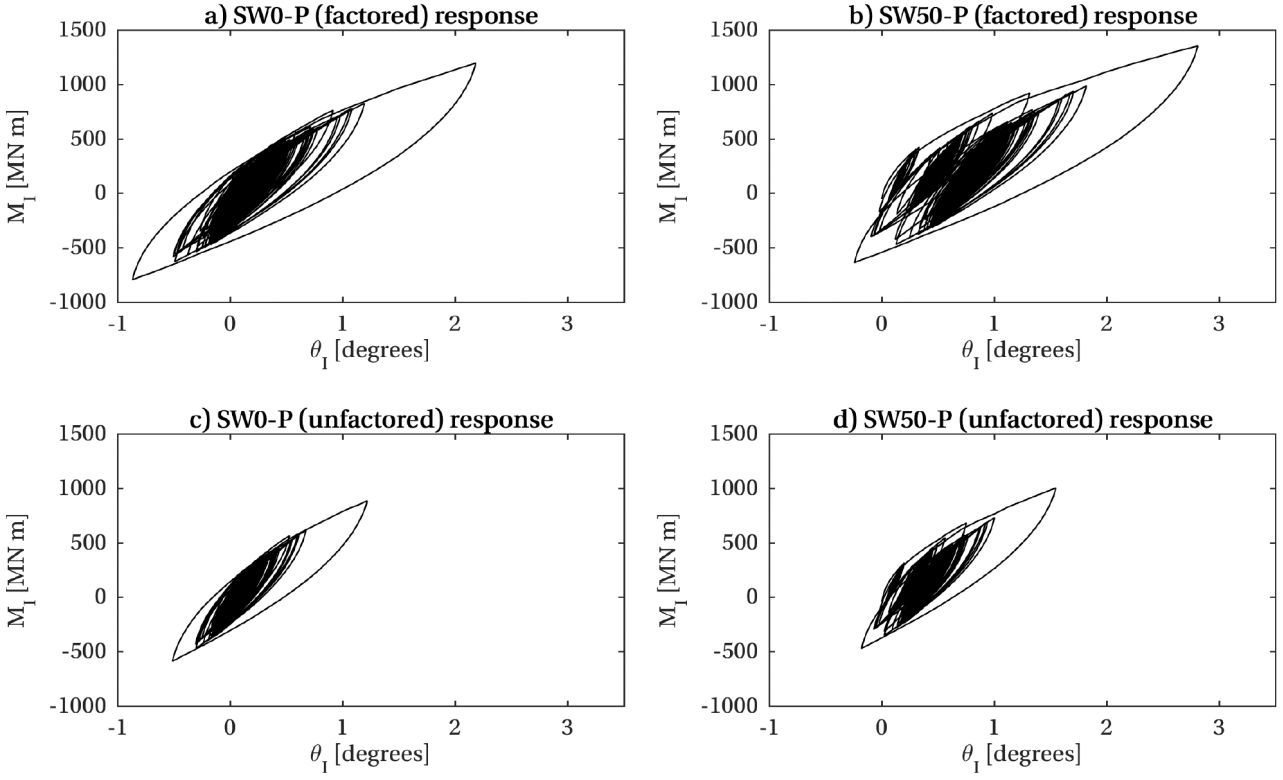

Fig. 10. Prediction of prototype scale monopile response to storm loading, using kinematic hardening model.

10 Conclusions

This paper presents a methodology which shows how laboratory scale testing can inform model development and prediction of the response of a monopile at prototype scale, when coupled with appropriate scaling methods. Laboratory tests as part of the DeRisk project allow accurate measurement of wave loads on a model monopile, while geotechnical laboratory scale tests allow the rotation response of the model monopile to be investigated. Processing of the DeRisk loads highlights the importance of structural dynamics in controlling load amplitude and number of cycles.

The response of the laboratory scale monopile is dominated by large load events and supports the use of kinematic hardening models. A basic kinematic hardening model is shown to predict the peak response reasonably well, but permanent rotation (ratcheting) is underestimated, particularly where additional wind loading is applied. More advanced models, such as described by Houlsby et al. (2017), are necessary to capture the ratcheting behaviour. Predictions at prototype scale suggest that extreme storm loading (with wind) would cause transient peak rotation of 1.5° for a 6.6 m diameter, 26.4 m long monopile in dense, fully drained sand.

This paper also demonstrates the benefits of inter-disciplinary work and data-sharing. The complex problem of OWT foundations under cyclic loading requires a number of different techniques to be combined and applied to provide input to design methods.

Acknowledgements

This work was supported by grant EP/L016303/1 for Cranfield University, the University of Oxford and Strathclyde University, Centre for Doctoral Training in Renewable Energy Marine Structures (REMS) from the UK Engineering and Physical Sciences Research Council (EPSRC). The wave data used in this paper came from the DeRisk project, funded by Innovation Fund Denmark. Input from Professor Tom Adcock and Dr Mark McAllister is gratefully acknowledged.

References

Abadie, C.N., Byrne, B.W. & Houlsby, G.T., 2018. Rigid pile response to cyclic lateral loading: laboratory tests. Géotechnique (ahead of print).

Abadie, C.N., Houlsby, G.T. & Byrne, B.W., 2019. A method for calibration of the Hyperplastic Accelerated Ratcheting Model (HARM). Computers and Geotechnics 112, 370-385. .

Achmus, M., Kuo, Y.S. & Abdel-Rahman, K., 2009. Behavior of monopile foundations under cyclic lateral load. Computers and Geotechnics, 36(5), 725–735.

Bachynski, E.., Kristiansen, T. & Thys, M., 2017. Experimental and numerical investigations of monopile ringing in irregular finite-depth water waves. Applied Ocean Research, 68, 154–170.

Bayton, S.M., Black, J.A. & Klinkvort, R.T., 2018. Centrifuge modelling of long term cyclic lateral loading on monopiles. In Proceedings of the 9th International Conference on Physical Modelling in Geotechnics. London, UK, 689–694.

Beuckelaers, W.J.A.P., 2017. Numerical Modelling of Laterally Loaded Piles for Offshore Wind Turbines, DPhil thesis, University of Oxford.

Bolton, M.D., 1987. Discussion on: The strength and dilatancy of sands, Bolton (1986). Géotechnique, 37(2), 219–226.

Bolton, M.D., 1986. The strength and dilatancy of sands. Géotechnique, 36(1), 65–78.

Bredmose, H. et al., 2016. DeRisk - Accurate Prediction of ULS Wave Loads. Outlook and First Results. Energy Procedia, 94, 379–387.

Houlsby, G.T., Abadie, C.N., Beuckelaers, W.J.A.P. & Byrne, B.W., 2017. A model for nonlinear hysteretic and ratcheting behaviour. International Journal of Solids and Structures, 120, 67–80.

Jeanjean, P. et al., 2017. A framework for monotonic p-y curves in clays. In Proceedings of the 8th International Conference on Offshore Site Investigation and Geotechnics (SUT). London, UK.

Kelly, R.B., Byrne, B.W. & Houlsby, G.T., 2006. A comparison of field and laboratory tests of caisson foundations in sand and clay. Géotechnique, 56(9), 617–626.

Klinkvort, R. & Hededal, O., 2013. Lateral response of monopile supporting an offshore wind turbine. Proceedings of the Institution of Civil Engineers - Geotechnical Engineering, 166(2), 147–158.

Leblanc, C., Houlsby, G.T. & Byrne, B.W., 2010. Response of stiff piles in sand to long-term cyclic lateral loading. Géotechnique, 60(2), 79–90.

Nguyen-Sy, L. & Houlsby, G. T., 2005. The theoretical modelling of a suction caisson foundation using hyperplasticity theory. In Proceedings of the International Symposium on Frontiers in Offshore Geotechnics. Perth, Australia.

Page, A., Grimstad, G., Eiksund, G. & Jostad, H., 2018. A macro-element pile foundation model for integrated analyses of monopile-based offshore wind turbines. Ocean Engineering, 167, 23-35.

Puzrin, A.M. & Houlsby, G.T., 2001. Fundamentals of kinematic hardening hyperplasticity. International Journal of Solids and Structures, 38(21), 3771–3794.
Richards, I.A., Byrne, B.W. & Houlsby, G.T., 2019a. Monopile rotation under complex cyclic lateral loading in sand. Manuscript submitted for publication.
Richards, I.A. et al., 2019b. The effect of stress-level on the response of a model monopile to cyclic lateral loading in sand. Unpublished manuscript.
Richards, I.A., Byrne, B.W. & Houlsby, G.T., 2018. Physical modelling of monopile foundations under variable cyclic lateral loading. In Proceedings of the 9th Int. Conf. on Physical Modelling in Geotechnics. London, UK, 737–742.
Schnaid, F., 1990. A study of the cone-pressuremeter test in sand, DPhil thesis, University of Oxford.
Sørensen, S.P.H., et al., 2017. Consequences of p-y curve selection for monopile design for offshore wind turbines. In Proceedings of the 8th Int. Conf. on Offshore Site Investigation and Geotechnics (SUT), 1062-1069. London, UK.
Tatsuoka, F. et al., 1986. Strength and deformation characteristics of sand in plane strain compression at extremely low pressures. Soils and Foundations, 26(1), 65–84.
Truong, P. et al., 2019. Empirical approach based on centrifuge testing for cyclic deformations of laterally loaded piles in sand. Geotechnique, 69(2), 133–145.
Wang, S., 2018. Assessment of offshore wind turbines in extreme weather conditions. PhD Thesis, DTU Wind Energy.
White, J.R.F., 2020. A laboratory investigation into the behaviour of sand at low confining stresses, forthcoming DPhil thesis, University of Oxford.
Wind Europe, 2018. Offshore Wind in Europe: Key trends and statistics 2017.